DOI: 10.1113/JP277443

Inspiratory pressure-generating capacity is preserved during ventilatory and non-ventilatory behaviours in young dystrophic *mdx* mice despite profound diaphragm muscle weakness

David P. Burns, Kevin H. Murphy, Eric F. Lucking and Ken D. O'Halloran*

Department of Physiology, School of Medicine, College of Medicine and Health, University College Cork, Cork, Ireland.

***Corresponding author:**

Professor Ken D. O'Halloran, PhD | Department of Physiology, Western Gateway Building, Western Road, Cork, Ireland | Tel: +353-21-4205433 | k.ohalloran@ucc.ie

Short title: Respiratory compensation in young *mdx* mice.

Abbreviations: ½ RT, half-relaxation time; ANOVA, analysis of variance; CSA, cross-sectional area; CT, contraction time; DMD, Duchenne muscular dystrophy; EIC, external intercostal; EMG, electromyogram; $ETCO_2$, end-tidal carbon dioxide; f_R, respiratory frequency; F_iO_2, fractional inspired oxygen concentration; L_o, optimum length; PIF, peak inspiratory flow; PEF, peak expiratory flow; P_t, twitch force; P_o, tetanic force; Smax, maximum total shortening; SpO_2, peripheral capillary oxygen saturation; T3, third intercostal space; V_E, minute ventilation; Vmax, maximum shortening velocity; V_T, tidal volume; V_T/T_i, mean inspiratory flow; WT, wild-type.

Key points

- Respiratory muscle weakness is a major feature of Duchenne muscular dystrophy (DMD), yet little is known about the neural control of the respiratory muscles in DMD and animal models of dystrophic disease.
- Substantial diaphragm muscle weakness is apparent in young (8-week-old) *mdx* mice, but ventilatory capacity in response to maximum chemostimulation in conscious mice is preserved.
- Peak volume- and flow-related measures during chemoactivation are equivalent in anaesthetized, vagotomized wild-type and *mdx* mice.

- Diaphragm and T3 external intercostal EMG activities are lower during protracted sustained airway occlusion in *mdx* compared with wild-type mice. Yet, peak inspiratory pressure generation is remarkably well preserved.
- Despite profound diaphragm weakness and lower muscle activation during maximum non-ventilatory efforts, inspiratory pressure-generating capacity is preserved in young adult *mdx* mice*,* revealing compensation in support of respiratory system performance that is adequate, at least early in dystrophic disease.

Abstract

Diaphragm dysfunction is recognized in the *mdx* mouse model of muscular dystrophy, however there is a paucity of information concerning the neural control of dystrophic respiratory muscles. In young adult (8 weeks of age) male wild-type and *mdx* mice, we assessed ventilatory capacity, neural activation of the diaphragm and external intercostal (EIC) muscles and inspiratory pressure-generating capacity during ventilatory and non-ventilatory behaviours. We hypothesized that respiratory muscle weakness is associated with impaired peak inspiratory pressure-generating capacity in *mdx* mice. Ventilatory responsiveness to hypercapnic hypoxia was determined in conscious mice by whole-body plethysmography. Diaphragm isometric and isotonic contractile properties were determined *ex vivo*. In anaesthetized mice, thoracic oesophageal pressure, and diaphragm and EIC electromyogram (EMG) activities were recorded during baseline conditions and sustained tracheal occlusion for 30-40s. Despite substantial diaphragm weakness, *mdx* mice retain the capacity to enhance ventilation during hypercapnic hypoxia. Peak volume- and flow-related measures were also maintained in anaesthetized, vagotomized *mdx* mice. Peak inspiratory pressure was remarkably well preserved during chemoactivated breathing, augmented breaths, and maximal sustained efforts during airway obstruction in *mdx* mice. Diaphragm and EIC EMG activities were lower during airway obstruction in *mdx* compared with wild-type mice. We conclude that ventilatory capacity is preserved in young *mdx* mice. Despite profound respiratory muscle weakness and lower diaphragm and EIC EMG activities during high demand in *mdx* mice, peak inspiratory pressure is preserved, revealing adequate compensation in support of respiratory system performance, at least early in dystrophic disease. We suggest that a progressive loss of compensation during advancing disease, combined with diaphragm dysfunction, underpins the development of respiratory system morbidity in dystrophic diseases.

Keywords: DMD; *mdx*; breathing; oesophageal pressure; EMG; diaphragm; intercostal

1. Introduction

Dystrophin is a structural protein expressed in muscle and the central nervous system (Lidov, 1996; Muntoni *et al.*, 2003). Duchenne muscular dystrophy (DMD) is a severe neuromuscular disease caused by dystrophin deficiency (Hoffman *et al.*, 1987; Ervasti, 2007). Respiratory muscle dysfunction is described in DMD patients (De Bruin *et al.*, 1997; Beck *et al.*, 2006) with deleterious consequences for respiratory system performance (Mayer *et al.*, 2015). Loss of ambulation and cardio-respiratory failure are cardinal features of DMD (Yiu & Kornberg, 2008). Life expectancy for DMD boys is severely curtailed and there is currently no cure for the devastating disease.

Substantial diaphragm muscle weakness is reported in patients and animal models of DMD (Stedman *et al.*, 1991; Khirani *et al.*, 2014). However, there remains an incomplete understanding of the neural control of breathing in DMD and dystrophic animal models, where further deficits or compensation may arise with implications for respiratory performance (Burns *et al.*, 2017c). A thorough understanding of the consequences of dystrophin deficiency for the control of breathing is essential in the consideration of disease progression and therapeutic strategies to combat respiratory insufficiency in human dystrophinopathies.

Dystrophin is ordinarily expressed in neurons (Lidov, 1996). In the *mdx* mouse model of DMD, studies indicate reduced number of cortico-spinal neurons (Sbriccoli *et al.*, 1995), damage to motor pathways (Carretta *et al.*, 2001), loss of neuronal projections (Pinto *et al.*, 2008), GABAergic dysfunction (Sekiguchi *et al.*, 2009; Vaillend & Chaussenot, 2017) and cognitive deficits (Chaussenot *et al.*, 2015). It is unclear if dystrophin deficiency affects nervous system control of breathing. A comprehensive understanding of the motor control of the dystrophin deficient respiratory musculature is lacking. It is essential to determine if dystrophin deficiency is deleterious to the motor control of breathing and respiratory-related behaviours, or if there is intrinsic compensation within the neural control circuits, facilitating performance. Recently, we described evidence of enhanced motor drive to the *mdx* diaphragm during chemoactivation of breathing (Burns *et al.*, 2017c), suggesting intrinsic compensation in the neural control of ventilation in dystrophin deficient mice. Our studies have revealed a retained capacity to increase ventilation in response to modest chemostimulation in young *mdx* mice (Burns *et al.*, 2017c). However, the extent to which dystrophin deficiency affects inspiratory pressure-generating capacity across a range of ventilatory and non-ventilatory behaviours (Mantilla *et al.*, 2010; Seven *et al.*, 2014) is unclear, but important to establish. Clearly, aberrant neural control of breathing could serve to exacerbate respiratory morbidity in DMD, compounding mechanical constraints arising from respiratory muscle dysfunction.

Our principal objective was to perform an assessment of respiratory system performance during ventilatory and non-ventilatory behaviours in the *mdx* mouse model of DMD. We assessed ventilatory capacity during hypercapnic hypoxic breathing in conscious mice. In anaesthetized mice, we determined inspiratory pressure-generating capacity and diaphragm and external intercostal (EIC) electromyogram (EMG) activities during ventilatory (chemoactivation and augmented breaths) and non-ventilatory (airway obstruction) behaviours. We hypothesized that respiratory muscle weakness is associated with impaired peak inspiratory pressure-generating capacity in *mdx* mice.

2. Methods

2.1 Ethical approval

Procedures on live animals were performed under licence in accordance with Irish and European law following approval by University College Cork animal research ethics committee (AEEC no. 2013/035). Experiments were carried out in accordance with guidelines laid down by University College Cork Animal Welfare Body, and conform to the principles and regulations described by Grundy (2015).

2.2 Experimental animals

Male wild-type (C57BL/10ScSnJ; n=28) and *mdx* (C57BL/10ScSn-Dmd^{mdx}/J; n=26) mice were purchased from the Jackson Laboratory (Bar Harbor, ME, USA) and studied at eight weeks of age. Animals were housed in individually ventilated cages in our institution's animal housing facility. All animals were housed in temperature- and humidity-controlled rooms, operating on a 12 h light:12 h dark cycle with food and water available *ad libitum*.

2.3 Whole-body plethysmography

Whole-body plethysmography was used to assess respiratory flow in unrestrained, unanaesthetized mice. Mice were introduced into plethysmograph chambers (Model PLY4211; volume 600ml, Buxco Research Systems, Wilmington, NC, USA) and allowed 60-90 min to acclimate to the chamber environment. Following exploration and grooming behaviours, mice settled and were studied during quiet rest. Recordings were typically performed contemporaneously in a wild-type and *mdx* mouse using a pair of plethysmograph chambers.

Experimental protocol: Following acclimation and a settling period, a 20-min baseline recording was performed in normoxia. This was followed by a graded hypercapnic challenge wherein animals were challenged with increasing levels of inspired carbon dioxide: F_iCO_2 = 0.02, 0.04 and 0.06 (F_iO_2 = 0.21) consecutively for 5 min each. This was immediately followed by maximal chemoreceptor stimulation

with hypercapnic hypoxia (F_iO_2 = 0.10/ F_iCO_2 = 0.06) for 5 min, to examine ventilatory capacity in wild-type (n = 9) and *mdx* (n = 7) mice. Mice were subsequently euthanized by urethane overdose.

Data analysis: Ventilation during hypercapnia and hypercapnic hypoxia was determined during steady-state conditions in the 5th minute of exposure and compared with the preceding baseline normoxic period. Tidal volume (V_T), minute ventilation (V_E) and mean inspiratory flow ($V_T.T_i^{-1}$) were normalized for body mass (g).

2.4 Diaphragm EMG and oesophageal pressure recordings

Anaesthesia was induced with 5% isoflurane in 60% O_2 (balance N_2) followed by urethane (1.7g.kg^{-1} i.p.). Wild-type (n = 9) and *mdx* (n = 9) mice were then placed in the supine position, gradually weaned from the isoflurane and body temperature was maintained at 37^{o}C via a rectal probe and thermostatically-controlled heating blanket (Harvard Apparatus, Holliston, MA, USA). Supplemental anaesthetic was administered if necessary to maintain an adequate surgical plane of anaesthesia, which was by assessment of pedal withdrawal reflex to noxious pinch. A pulse oximeter clip (MouseOx^{TM}, Starr Life Sciences Corporation, Oakmount, PA, USA) was placed on a shaved thigh of each mouse for the measurement of peripheral capillary O_2 saturation (SpO_2). A mid-cervical tracheotomy was performed. All animals were maintained with a bias flow of supplemental O_2 (FiO_2 = 0.60) under baseline conditions. End-tidal carbon dioxide ($ETCO_2$) was measured using a MicroCapStar (CWE, Ardmore, PA). To estimate intra-pleural sub-atmospheric pressure generated by the respiratory musculature during inspiration, we measured oesophageal pressure using a pressure-tip catheter (Mikro-Tip, Millar Inc., Houston, TX, USA), which was positioned in the thoracic oesophagus through the mouth. During inspiratory activity, oesophageal recordings displayed phasic sub-atmospheric pressure swings. Concentric needle electrodes (26G; Natus Manufacturing Ltd, Ireland) were inserted into the costal diaphragm for the continuous measurement of diaphragm EMG activity, which was amplified (x5,000), filtered (500Hz low cut-off to 5,000Hz high cut-off) and integrated (50ms time constant; Neurolog system, Digitimer Ltd, UK). All signals were passed through an analogue-to-digital converter (Powerlab r8/30; ADInstruments, Colorado Springs, CO, USA) and were acquired using LabChart 7 (ADInstruments).

Experimental protocol: Following instrumentation, animals were allowed at least 10 min to stabilize before baseline parameters were measured for a period of 10 min. Next, animals were challenged with hypercapnic hypoxia (F_iO_2 = 0.15 & F_iCO_2 = 0.05; 1 min) to examine the effects of chemostimulation on diaphragm EMG activity and oesophageal inspiratory pressure generation.

Following the experimental protocol, mice were euthanized by decapitation. Diaphragm muscle was excised for *ex vivo* functional analysis (section 2.6).

Data analysis: The amplitudes of integrated inspiratory diaphragm EMG activity and peak inspiratory sub-atmospheric oesophageal pressure were analyzed and averaged under steady-state basal conditions and averaged for the final 15 breaths (maximal response) of the hypercapnic hypoxia challenge. Oesophageal pressure is reported in absolute units (cmH_2O). EMG data are reported in arbitrary units (A.U.). In one wild-type and three *mdx* mice, responses to chemostimulation were characterized by tachypnoea and a reduction in EMG amplitude. Since, our aim was to examine the magnitude of the increase in EMG amplitude (motor recruitment) of the diaphragm during maximal chemoreceptor stimulation with hypercapnic hypoxia we determined *a priori* that trials characterized by frequency-only responses to gas challenge in wild-type and *mdx* mice would be excluded from group analysis, consistent with our approach in a recent study (Burns *et al.*, 2017c). Spontaneous augmented breaths (sighs) observed during baseline conditions were analyzed and compared with the average of the preceding five breaths. Augmented breaths were classified as breaths with more than double the baseline EMG amplitude (Mantilla *et al.*, 2011; Seven *et al.*, 2014). For two wild-type mice, no breath met this criterion during the recording period.

2.5 Diaphragm and EIC EMG and oesophageal pressure recordings

In separate studies, wild-type (n=10) and *mdx* (n=10) mice were anaesthetized and tracheotomized as described above (section 2.4). Oesophageal pressure and costal diaphragm EMG activity were recorded. In addition, a concentric needle electrode was inserted in the third intercostal space (T3) for the measurement of EIC EMG, which was amplified (x5,000), filtered (500Hz low cut-off to 5,000Hz high cut-off) and integrated (50ms time constant; Neurolog system, Digitimer Ltd, UK). All signals were passed through an analogue-to-digital converter and were acquired using LabChart 7.

Experimental protocol: Following instrumentation, animals were allowed at least 10 min to stabilize before baseline parameters were measured for a period of 10 min. Next, a pneumotachometer was connected to the tracheal cannula to record respiratory airflow for a period of 1-2 min. The pneumotachometer and $ETCO_2$ were disconnected and following a baseline period, animals were challenged with sustained tracheal occlusion for 30-40s until a plateau was observed in the inspiratory pressure recordings during sustained maximum non-ventilatory efforts. Following recovery, animals were instrumented for the measurement of $ETCO_2$ and tracheal airflow and the vagi were sectioned bilaterally at the cervical level. Respiratory parameters were recorded for 10 min under steady-state conditions following vagotomy. Next, animals were challenged with

hypercapnic hypoxia (F_iO_2 = 0.15 & F_iCO_2 = 0.06; 3 min) to examine the effects of chemostimulation on diaphragm and EIC EMG activities and tracheal airflow. Following the experimental protocol, mice were euthanized by decapitation.

Data analysis: The amplitudes of integrated inspiratory diaphragm and EIC EMG activities and peak inspiratory sub-atmospheric oesophageal pressure were analyzed and averaged under steady-state basal conditions and averaged for the 5 successive maximal sustained efforts (maximal response) of the airway occlusion challenge. During baseline breathing and chemoactivation, V_T was derived from tracheal airflow measurements. Spontaneous peak breaths observed during chemoactivation in vagotomized mice, notably greater in amplitude than neighbouring breaths, were analyzed and compared with the preceding baseline period to provide a measure of maximum ventilatory effort. Spontaneous peak breaths during hypercapnic hypoxia were observed in 5 wild-type and 5 *mdx* mice and were analyzed as a measure of peak ventilatory performance.

2.6 Ex vivo *diaphragm muscle function*

Diaphragm muscle was excised with a rib and central tendon attached. Muscle bundles with longitudinally arranged muscle fibres were prepared for functional assessment and suspended vertically between two platinum plate electrodes. The rib was attached to an immobile hook and the central tendon was attached to a dual-mode force transducer (Aurora Scientific Inc.; Aurora, ON, Canada) with non-elastic string. Diaphragm muscle preparations from wild-type (n = 8) and *mdx* (n = 9) mice were studied in a water-jacketed tissue bath at 35^{o}C containing Krebs solution (in mM: 120 NaCl, 5 KCl, 2.5 Ca^{2+}, 1.2 $MgSO_4$, 1.2 NaH_2PO_4, 25 $NaHCO_3$, 11.5 glucose) and D-tubocurarine (25 μM) and were continuously aerated with carbogen (F_iO_2 = 0.95 & F_iCO_2 = 0.05). Muscle optimum length (L_o) was determined by adjusting the position of the force transducer, in turn adjusting the length of the muscle preparations, using a micro-positioner between intermittent twitch contractions (Burns & O'Halloran, 2016; Burns *et al.*, 2017b). L_o was determined as the muscle length which revealed maximal isometric twitch force in response to single isometric twitch stimulation (supramaximal stimulation, 1ms duration). Preparations remained at L_o for the duration of the protocol.

Experimental protocol: A single isometric twitch contraction was measured. Peak isometric twitch force (P_t), contraction time (CT) and half-relaxation time (½ RT) were determined. Peak isometric force at 100Hz (P_o) was determined. The force-frequency relationship was examined by stimulating the muscle sequentially at 10, 20, 40, 60, 80, 100, 120, 140 and 160 Hz (300ms train duration). Contractions were interspersed by a 1 min interval. Next, an isotonic contraction was elicited in

preparations at 0% load to examine maximum unloaded muscle shortening and velocity of shortening (Burns & O'Halloran, 2016; Burns *et al.*, 2017b).

Data analysis: Muscle force was normalized for muscle cross-sectional area (CSA) and expressed as specific force (N cm^{-2}). The CSA of each muscle bundle was determined by dividing muscle mass (weight in grams) by the product of muscle L_o (cm) and muscle density (assumed to be 1.06 g cm^{-3}). CT and ½ RT were measured as indices of isometric twitch kinetics. Total muscle shortening was determined as the maximum distance shortened during contraction. Total muscle shortening (Smax) was determined in absolute units (cm) and was normalized to L_o and expressed in $L.L_o^{-1}$. Shortening velocity was determined as the distance shortened during the initial 30 ms of shortening (Lewis *et al.*, 2015; 2016). Shortening velocity (Vmax) was determined in absolute units ($cm.s^{-1}$) and was normalized to L_o and expressed in $L_o.s^{-1}$.

2.7 Statistical analysis

Values are expressed as mean ± SD or as box and whisker plots (median, 25-75 percentile, and scatter plot). Data were statistically compared using Prism 6.0 (Graphpad Software, San Diego, CA, USA). Data were tested for normal distribution and equal variances. Data sets which were normally distributed and of equivalent variance were statistically compared using unpaired two-tailed Student's *t* test. Welch's correction was applied in the case of unequal variance. Data which were not normally distributed were compared using Mann Whitney non-parametric tests. Data for diaphragm muscle force-frequency relationship, ventilatory responsiveness to chemostimulation in conscious mice, oesophageal pressure and EMG activities during obstruction, and flow, volume and EMG measures during peak breaths in vagotomized mice during chemoactivation were statistically compared by repeated measures two-way ANOVA with Bonferroni *post hoc* test. $P < 0.05$ was considered statistically significant in all tests.

3. Results

3.1 Diaphragm muscle contractile function ex vivo

Figure 1 shows representative original recordings for wild-type (black) and *mdx* (grey) diaphragm twitch (A) and tetanic (B) contractions, force-frequency relationship (C) and maximal unloaded shortening (D). Twitch kinetics (CT and ½ RT) and isotonic contractile parameters (Smax and Vmax) are shown in Table 1. Twitch CT was significantly increased in *mdx* compared with wild-type diaphragm ($P = 0.027$; unpaired Student's *t* test). Twitch ½ RT and isotonic contractile parameters were not significantly different between wild-type and *mdx* diaphragm preparations, with the

exception of absolute shortening and absolute velocity of shortening, which were significantly less in *mdx* compared with wild-type mice (Table 1). Diaphragm twitch (P = 0.0241; unpaired Student's t test; Fig. 1E, P_t) and tetanic force (P < 0.0001; unpaired Student's t test with Welch's correction; Fig. 1E, P_o) were both significantly depressed in *mdx* compared with wild-type muscle. For the force-frequency relationship, diaphragm specific force was significantly lower in *mdx* compared with wild-type preparations (P = 0.0003 (genotype); repeated measures two-way ANOVA; Fig. 1F). *Post hoc* analysis confirmed significant force depression in *mdx* across a broad range of stimulation frequencies (60-160 Hz).

3.2 Ventilatory responsiveness to hypercapnic hypoxia in conscious mice

Figure 2A shows representative respiratory flow traces for wild-type and *mdx* mice during exposure to baseline air (F_iO_2 = 0.21) and hypercapnic hypoxia (F_iO_2 = 0.10 & F_iCO_2 = 0.06). Chemostimulation with graded hypercapnia and hypercapnic hypoxia resulted in a significant increase in f_R (P < 0.0001 (gas); repeated measures two-way ANOVA; Fig. 2B), V_T (P < 0.0001; Fig. 2C), V_E (P < 0.0001; Fig. 2D) and $V_T.T_i^{-1}$ (P < 0.0001; Fig. 2E) both for wild-type and *mdx* mice, with no difference between the two groups.

3.3 Oesophageal pressure and diaphragm EMG activity in anaesthetized mice

Representative original recordings of oesophageal pressure and diaphragm EMG during baseline conditions (F_iO_2 = 0.60) and during a representative spontaneous augmented breath (shaded) are shown in Figure 3A. Table 2 shows baseline respiratory measurements in wild-type and *mdx* mice. Respiratory frequency was significantly higher in *mdx* compared with wild-type mice (P < 0.0001; unpaired Student's t test; Table 2). There was no significant difference in SpO_2 and $ETCO_2$ between wild-type and *mdx* mice (Table 2).

Peak inspiratory oesophageal pressure during baseline recordings was equivalent between wild-type and *mdx* mice (P = 0.2887; unpaired Student's t test; Fig. 3B). Baseline diaphragm EMG activity was significantly lower in *mdx* (P = 0.025; unpaired Student's t test with Welch's correction; Fig. 3C) compared with wild-type mice. The peak inspiratory pressure generated during chemoactivation (F_iO_2 = 0.15 & F_iCO_2 = 0.05) was equivalent in wild-type and *mdx* mice, with a trend towards greater sub-atmospheric pressure generation in *mdx* mice (P = 0.0563; unpaired Student's t test; Fig. 3B). Diaphragm EMG activity during chemoactivation was not different between wild-type and *mdx* mice (P = 0.0853; unpaired Student's t test with Welch's correction; Fig. 3C). Peak inspiratory oesophageal pressure during augmented breaths was greater in *mdx* compared with wild-type mice (P = 0.0013;

unpaired Student's *t* test; Fig. 3B). Diaphragm EMG during augmented breaths was equivalent between wild-type and *mdx* mice ($P = 0.2031$; unpaired Student's *t* test; Fig. 3C).

3.4 Oesophageal pressure and diaphragm and EIC EMGs during airway obstruction in anaesthetized mice

Representative original recordings of oesophageal pressure, diaphragm and EIC EMG activities during baseline conditions ($F_iO_2 = 0.60$) and peak sustained inspiratory efforts during protracted airway obstruction are shown in Figure 4A and 4B. Obstruction significantly increased sub-atmospheric pressure generation in wild-type ($P < 0.0001$; repeated measures two-way ANOVA with Bonferroni; Fig. 5A) and *mdx* mice ($P < 0.0001$; Fig. 5A), with no significant difference between the two groups ($P = 0.1931$ (gene); repeated measures two-way ANOVA; Fig. 5A). Diaphragm EMG activity was significantly increased during airway obstruction compared with baseline in wild-type ($P < 0.0001$; repeated measures two-way ANOVA with Bonferroni; Fig. 5B) and *mdx* mice ($P < 0.001$). However, diaphragm EMG activity was lower in *mdx* ($P = 0.0479$ (gene); repeated measures two-way ANOVA; Fig. 5B) and *mdx* mice had significantly lower diaphragm EMG activity compared with wild-type during airway obstruction ($P < 0.05$; repeated measures two-way ANOVA with Bonferroni; Fig. 5B). Airway obstruction significantly increased EIC EMG activity in wild-type ($P < 0.0001$; repeated measures two-way ANOVA with Bonferroni; Fig. 5C), but not *mdx* mice ($P > 0.05$). EIC EMG activity was lower in *mdx* compared with wild-type ($P = 0.0003$ (gene); repeated measures two-way ANOVA; Fig. 5C). *Post hoc* analysis revealed that EIC EMG activity was significantly lower during airway obstruction in *mdx* compared with wild-type mice ($P < 0.0001$; repeated measures two-way ANOVA with Bonferroni; Fig. 5C). In the light of these findings, we extended our analyses to determine inspiratory duration and respiratory EMG activities expressed as area under the curve (AUC) of the integrated EMG signals before and during airway obstruction (Table 3). During baseline recordings, inspiratory duration was shorter in *mdx* compared with wild-type mice ($P < 0.05$; repeated measures two-way ANOVA with Bonferroni). Inspiratory duration was significantly longer during obstructed airway efforts, both in wild-type and *mdx* mice, with no genotype difference. Consistent with data for respiratory EMG amplitude during airway obstruction, both diaphragm ($P < 0.05$) and EIC ($P < 0.001$) EMG AUC activities were significantly lower in *mdx* compared with wild-type mice (Table 3).

3.5 Tracheal airflow and diaphragm and EIC EMG activity in anaesthetized, vagotomized mice

Table 4 shows respiratory data in anaesthetized, vagotomized wild-type and *mdx* mice during baseline conditions ($F_iO_2 = 0.60$). There was no significant difference in f_R, V_T or V_E between wild-type and *mdx* mice. Similarly, peak inspiratory and expiratory flows, and $ETCO_2$ and SpO_2 were equivalent

between groups. Figure 6A shows representative original recordings of tracheal airflow, diaphragm and EIC EMG activities in anaesthetized, vagotomized mice during baseline conditions (F_iO_2 = 0.60). Peak respiratory efforts during chemoactivation increased V_T (P < 0.0001 (peak breath); repeated measures two-way ANOVA; Fig. 6B), peak inspiratory flow (P = 0.027; Fig. 6C) and peak expiratory flow (P = 0.016; Fig. 6D), with no difference between wild-type and *mdx* mice. Diaphragm EMG activity increased during peak respiratory efforts (P = 0.0128 (peak breath); repeated measures two-way ANOVA; Fig. 6E) in wild-type and *mdx* mice, with equivalent diaphragm EMG activity between groups (P = 0.4055 (gene); repeated measures two-way ANOVA; Fig. 6E). Diaphragm EMG recruitment (delta EMG amplitude) during peak respiratory efforts compared with baseline was equivalent between wild-type and *mdx* (P = 0.9953; unpaired Student's *t* test; Fig. 6F). EIC EMG activity was significantly lower during baseline conditions in *mdx* mice compared with wild-type (P < 0.05; repeated measures two-way ANOVA with Bonferroni; Fig. 6G) and during peak chemoactivation (P < 0.01). EIC EMG recruitment (delta EMG amplitude) during peak ventilation compared with baseline was significantly lower in *mdx* compared with wild-type mice (P = 0.0434; unpaired Student's *t* test; Fig. 6H).

4. Discussion

The main findings of the study are: (i) there is substantial diaphragm muscle weakness in young adult *mdx* mice; (ii) ventilatory capacity in response to maximum chemostimulation is equivalent between conscious wild-type and *mdx* mice; (iii) peak tidal volume and peak inspiratory and expiratory flows during maximum chemoactivation are equivalent in anaesthetized, vagotomized wild-type and *mdx* mice; (iv) peak inspiratory pressure-generating capacity is preserved in *mdx* mice during ventilatory (chemoactivated breathing and augmented breaths) and non-ventilatory (sustained tracheal occlusion) behaviours; (v) diaphragm and EIC EMG activities are lower during airway obstruction in *mdx* compared with wild-type mice.

Our study confirmed substantial diaphragm muscle weakness in young adult *mdx* mice, consistent with our recent reports (Burns *et al.*, 2017a,c). Diaphragm deficits in *mdx* mice were evidenced by significantly reduced twitch and tetanic isometric force compared with wild-type. The force-frequency relationship revealed considerable force loss in the frequency range of 60-160 Hz, corresponding to a broad range of ventilatory and non-ventilatory behaviours (Sieck *et al.*, 2013; Mantilla *et al.*, 2014). We have previously documented considerable muscle fibre damage and remodelling in dystrophic diaphragm at this age, with increased variability of muscle fibre size, centralized myonuclei, altered myosin heavy chain isoform composition, and collagen deposition

(Burns *et al.*, 2017c, 2018). Force loss was accompanied by decreases in muscle shortening and velocity of shortening.

Notwithstanding the profound diaphragm weakness in *mdx*, we reasoned that ventilatory behaviours might be protected owing to the large reserve capacity of the diaphragm muscle, such that maximum ventilation during chemoactivation can be achieved with <40% of peak diaphragm force (Sieck & Fournier, 1989; Mantilla *et al.*, 2010; Medina-Martínez *et al.*, 2015; Greising *et al.*, 2016). In contrast, we hypothesize that non-ventilatory behaviours such as airway obstruction, airway clearance, respiratory reflexes encompassing coughing and sneezing, requiring substantially elevated respiratory muscle activation, critical for the safeguarding of pulmonary function are compromised in dystrophic disease. Dysphagia and poor airway control increase the risk of obstructive airway events during sleep, which are common in teenage DMD boys (Barbé *et al.*, 1994; Khan & Heckmatt, 1994; Suresh *et al.*, 2005; Sawnani *et al.*, 2015). Peak respiratory pressures are low in DMD and are known to decline progressively with advancing disease (Khirani *et al.*, 2014).

We assessed ventilation in response to hypercapnic, and hypercapnic hypoxic challenges, which confirmed the capacity for *mdx* mice to enhance ventilation. Ventilation during graded hypercapnia was equivalent in *mdx* and wild-type mice, revealing that CO_2 chemosensitivity is intact in young adult *mdx* mice, which retain considerable ventilatory reserve and, despite diaphragm dysfunction, maintain a capacity to elevate V_E to wild-type levels, through increases in rate and volume. This preserved capacity to elevate pulmonary ventilation was further revealed during exposure to hypercapnic hypoxia with peak ventilation increasing more than 3-fold in *mdx* mice, equivalent to responses in wild-type mice. We acknowledge the limitations of accurate determination of tidal volume by the method of plethysmography, which may have been further limited in our study owing to our estimation (not continuous measurement) of body temperature.

In anaesthetized mice, we demonstrated that peak inspiratory oesophageal pressure generation was equivalent during basal breathing (F_iO_2 = 0.60) in *mdx* and wild-type mice. Acute chemoactivation (F_iO_2 = 0.15 & F_iCO_2 = 0.05) increased ventilatory drive and the magnitude of the enhanced peak inspiratory oesophageal pressure was equivalent in *mdx* and wild-type mice. This confirmed the lack of mechanical deficit in young adult *mdx* mice and hence no limitation in sub-atmospheric pressure-generating capacity during chemoactivation. Diaphragm EMG responses to hypercapnic hypoxia were equivalent in *mdx* compared with wild-type mice. As such, it is likely that even the compromised dystrophic *mdx* diaphragm is capable of supporting high ventilatory demand.

We extended this line of enquiry by way of assessment of spontaneous augmented breaths (sighs), which result in elevated diaphragm motor unit recruitment beyond that observed during chemoactivation (Mantilla *et al.*, 2011; Seven *et al.*, 2014), producing up to 50% of peak transdiaphragmatic pressure in mice (Greising *et al.*, 2013; 2015; 2016). Interestingly, during augmented breaths, peak inspiratory oesophageal pressure generation was preserved and significantly greater in *mdx* compared with wild-type mice, again convincingly demonstrating a lack of mechanical constraint in 8-week-old *mdx* mice despite substantial diaphragm weakness (approaching 50% force loss compared with wild-type in the range 60-100Hz). Of note, diaphragm EMG recruitment during spontaneous augmented breaths was equivalent (not potentiated) in *mdx* compared with wild-type mice. Thus, as is the case for ventilation during chemoactivation, augmented breaths are not compromised in young adult *mdx* mice, insofar as enhanced inspiratory pressures can be achieved even with 50% reduction in force-generating capacity of the diaphragm, presumably because such efforts either remain within the reserve capacity of the dystrophic diaphragm, or they are facilitated by accessory muscle recruitment, which can compensate for efforts exceeding the reserve capacity of the weakened *mdx* diaphragm. Of note in our study, inspiratory pressure generation during augmented breaths was greater in *mdx* compared with wild-type mice, but diaphragm EMG recruitment was equivalent between groups.

In addition, we examined tracheal airflow in anaesthetized, vagotomized mice during chemoactivation, wherein we characterized maximum ventilatory effort, exceeding that of volume-related measures in conscious mice owing to the release of vagal inhibition of breathing with superimposed chemoactivation of respiratory motor outflow. Direct measures of peak V_T and peak inspiratory and expiratory flows were equivalent in vagotomized wild-type and *mdx* mice, confirming and extending observations from our studies using plethysmography. Peak diaphragm EMG activity was equivalent in wild-type and *mdx* mice, whereas EIC EMG was significantly lower in *mdx* mice. Preserved neural drive to the weakened *mdx* diaphragm may be wholly adequate to generate even the large volumes and respiratory flows observed in vagotomized *mdx* mice. In this respect, our findings are consistent with a variety of other studies revealing that transdiaphragmatic pressure-generating capacity during high ventilatory demand (chemoactivation; augmented breaths) is within 50% of maximum capacity (Sieck & Fournier, 1989; Mantilla *et al.*, 2010), including studies in mice (Greising *et al.*, 2013, 2015, 2016), and these behaviours can be adequately met even in the context of motor neuron loss (Khurram *et al.*, 2018a) or age-related sarcopenia of the diaphragm (Khurram *et al.*, 2018b). Although force loss is severe in *mdx* diaphragm, ventilatory behaviours are accommodated, at least early in dystrophic disease.

Our consideration of respiratory-related capacity to this point was limited to peak ventilation during chemoactivation of breathing, albeit including observations in animals with removal of vagal afferent inhibition of respiratory drive. We reasoned that the preserved capacity in *mdx* might be limited to the ventilatory range, such that mechanical deficit might be revealed during non-ventilatory efforts, particularly over sustained periods, which evoke near-maximum respiratory system activation, or at least activation well beyond the reserve capacity of the weakened *mdx* diaphragm. To investigate this, we extended our studies to examine peak inspiratory pressure-generating capacity in wild-type and *mdx* mice during protracted sustained tracheal occlusion, which results in greater motor recruitment of respiratory muscles beyond that of augmented breaths (Mantilla *et al.*, 2011; Greising *et al.*, 2013; Seven *et al.*, 2014). Previously it has been shown that sustained tracheal occlusions lasting 15s in anaesthetized mice result in the generation of transdiaphragmatic pressures ~65-82% of peak pressures evoked by bilateral phrenic nerve stimulation (Greising *et al.*, 2013, 2015, 2016), with transdiaphragmatic pressure values of ~72cmH_20 during obstruction in young male mice, equating to ~78% of maximum transdiaphragmatic pressure (Greising *et al.*, 2015). In our study, oesophageal pressure recordings were performed in anaesthetized mice with contemporaneous measurement of diaphragm and EIC EMG activity. Tracheal occlusions sustained for 30-40s generated impressive sub-atmospheric inspiratory pressures in wild-type and *mdx* mice. The sustained efforts during the final phase of airway obstruction were likely reflective of maximum or near-maximum respiratory system performance, evidenced by progressively greater sub-atmospheric inspiratory pressures during occlusion to a sustained nadir associated with maximal diaphragm and EIC recruitment. Indeed, sub-atmospheric pressures were often noted to decrease further (become more 'negative') both in wild-type and *mdx* mice, when diaphragm EMG activity reached a maximum plateau or even decreased compared with preceding efforts.

Tracheal occlusion in our study resulted in sub-atmospheric pressure generation that clearly exceeded the reserve capacity of the dystrophic diaphragm. Moreover, both diaphragm and EIC EMG activities (determined both as amplitude and AUC of the integrated EMG signals) were substantially lower during peak sustained efforts in *mdx* compared with wild-type mice, with a relatively greater reduction of activity in EIC EMG compared with diaphragm EMG in *mdx* mice. Decreased EMG activity during airway obstruction could reflect impaired motor control of the diaphragm and EIC muscles, but is more likely fully explained by impaired neuromuscular transmission given the evidence in young *mdx* mice of increased variability of neural transmission to the diaphragm (Personius & Sawyer, 2006) and decreased amplitude of *mdx* diaphragm motor end plate potentials (Carlson & Roshek, 2001). Neuromuscular impairment during high demand behaviours that exceed the reduced reserve capacity of the *mdx* diaphragm would be expected to

translate to substantial inability to generate peak inspiratory pressures equivalent to wild-type, beyond that predicted by assessment of diaphragm peak force. However, in our study, peak sustained inspiratory pressures during airway obstruction were equivalent in wild-type and *mdx* mice. We determined that inspiratory duration, which is prolonged during obstructed efforts, was equivalent during peak sustained efforts in wild-type and *mdx* mice, highlighting that compensation in the capacity to generate equivalent sub-atmospheric pressures in *mdx* mice does not depend upon altered control of inspiratory timing. We therefore reason that recruitment of support muscles beyond the primary muscles of inspiration (diaphragm and EIC) contributes substantively to non-ventilatory pressure-generating capacity in young dystrophic *mdx* mice, owing to necessary and sufficient compensation that is capable of facilitating increased thoracic volume. It is clear from our study that T3 EIC muscle activity is severely curtailed in *mdx* mice, suggesting that intercostal muscles do not provide compensation during high demand behaviours in *mdx* mice. Of note, ventilatory capacity is maintained in rat models of amyotrophic lateral sclerosis (ALS) at end-stage disease despite substantial loss of phrenic motor neurons (Nichols *et al.*, 2013; Nichols *et al.*, 2014). Indeed, it is established that scalene and trapezius muscles enhance ventilation in ALS mice (Romer *et al*. 2017).

Elegant work in dystrophic dogs with the GRMD mutation showed a reduced diaphragm contribution to inspiratory tidal volume during wakefulness at rest in the lateral recumbent position (Mead *et al*. 2014). Moreover, there was loss of ventilatory capacity during pharmacological stimulation of breathing, but capacity is partly compensated for by expiratory muscles that serve to lower end-expiratory chest wall volume. The authors offer an excellent perspective on a proposed redistribution of the work of breathing beyond the diaphragm to accessory and auxiliary muscles in the context of dystrophic disease. Of further interest, a strong argument is also presented by Mead and colleagues (2014) in favour of viewing increased diaphragm stiffness as an adaptive benefit in muscular dystrophy (Mead *et al*. 2014), an outcome that may defend against cranial movement of the diaphragm during subatmospheric pressure generation by accessory and support muscles, particularly during high demand behaviours. Similar changes in the two-compartment chest wall model of breathing are reported in DMD patients (LoMauro *et al*. 2010), with outcomes dependent upon posture (lower diaphragm contribution to tidal volume in the supine position), but surprisingly not influenced by the presence or absence of scoliosis (LoMauro et al., 2010). It is plausible that expiratory muscle activation is increased in dystrophic disease in support of ventilatory capacity. Beyond the recognised contribution of active expiration to increased ventilatory capacity in support of inspiratory muscle work, expiratory muscle recruitment could serve to shorten expiratory duration and decrease end-expiratory lung volume, accessing expiratory reserve volume in

dystrophic animals and DMD boys allowing increases in tidal volume (Mead et al. 2014), until compensation is progressively lost with advancing disease.

In respect of the preserved capacity of *mdx* mice to generate peak inspiratory pressures during airway obstruction, we posit that auxiliary muscle recruitment in support of peak pressure-generating capacity offers the most plausible explanation for respiratory compensation in young *mdx* mice, notwithstanding that the muscle group(s) pivotal to the support of respiratory system compensation during non-ventilatory behaviours were not identified in the present study. Fibrosis in *mdx* (and DMD) leads to decreased chest wall compliance and increased work of breathing. Whereas the extent of fibrosis and its expected impact on chest wall compliance was not determined in the present study, and may not be a major pathology in young *mdx* mice, but with presumed greater relevance at later stages of disease, we reason that compensated inspiratory pressure-generating capacity in *mdx* mice does not relate to increased chest wall compliance. Indeed, compensation is likely limited by increased chest wall stiffness during progressive disease in *mdx* and DMD, adding further to the burden of a redistributed workload on accessory and auxiliary muscles.

The long-term compensatory capacity of primary and secondary respiratory motor pathways and muscles in *mdx* (and DMD) is not known. We speculate that in dystrophic disease there may be serial recruitment of accessory and other support muscles that facilitate respiratory performance, but in turn show progressive deterioration. Mechanical strain leads to injury in dystrophic muscle, triggering a spiral of progressive dysfunction. It is known, for example, that recruitment of the *mdx* diaphragm in exercise expedites diaphragm dysfunction (Capogrosso *et al.*, 2017). As such, the early modest decline in inspiratory pressure-generating capacity in *mdx* mice that we observed in our study (~10% loss comparing median values in Fig. 5A), could conceivably decline further with advancing disease. We suggest that compensation does not prevail during progressive dystrophic disease, a hypothesis previously suggested by others (Gayraud *et al.*, 2007). It is especially interesting to consider that peak hypercapnic ventilation is normal in 5-month old *mdx* mice (Gayraud *et al.*, 2007), but decreased at 7-months, 10-12 months (Gosselin *et al.*, 2003) and 16 months of age (Gayraud *et al.*, 2007). Interestingly, diaphragm dysfunction presents early in the *mdx* model, with relatively modest further deterioration in force-generating capacity with advancing disease (eg 50-66% force loss at 7-14 months of age: (Lynch *et al.*, 2001; Gosselin *et al.*, 2003; Selsby *et al.*, 2016). We therefore suggest that progressive decline in ventilatory performance in *mdx* (and perhaps DMD) potentially relates to an increased dependence upon, and progressive loss of compensatory mechanisms, which combined with diaphragm dysfunction underpins the development of respiratory morbidity. In DMD, there is a progressive decline in pulmonary function

and respiratory muscle strength culminating in reduced ventilation (Smith *et al.*, 1989; De Bruin *et al.*, 1997; Hukins & Hillman, 2000; Khirani *et al.*, 2014). The decline in peak respiratory pressure generation in DMD has important prognostic value (Phillips *et al.*, 2001; Khirani *et al.*, 2014).

In summary, our study highlights new facets to breathing with neuromuscular disease. We demonstrate profound diaphragm muscle weakness during early disease progression in young adult *mdx* mice, but a capacity to preserve ventilatory behaviours over a wide range. Ventilatory demand is likely adequately met by even the compromised dystrophic diaphragm, at least in early disease. We reveal the remarkable preservation of inspiratory pressure-generating capacity during sustained airway obstruction in *mdx* mice, which illustrates necessary and sufficient compensation within the respiratory control system. We hypothesize that there is an increased reliance on compensatory support, which is progressively lost in *mdx* (and DMD), which combined with devastating primary respiratory muscle (and neuromuscular junction) dysfunction contributes to respiratory-related morbidity culminating in the sequential loss of non-ventilatory and ventilatory capacity, ultimately leading to respiratory morbidity and failure in advanced disease. Our findings have relevance to human dystrophinopathies and therapeutic strategies for pulmonary support and rehabilitation in DMD boys.

5. References

Barbé F, Quera-Salva MA, McCann C, Gajdos P, Raphael JC, de Lattre J & Agustí AG. (1994). Sleep-related respiratory disturbances in patients with Duchenne muscular dystrophy. *Eur Respir J* **7,** 1403-1408.

Beck J, Weinberg J, Hamnegård CH, Spahija J, Olofson J, Grimby G & Sinderby C. (2006). Diaphragmatic function in advanced Duchenne muscular dystrophy. *Neuromuscul Disord* **16,** 161-167.

Burns DP, Ali I, Rieux C, Healy J, Jasionek G & O'Halloran KD. (2017a). Tempol Supplementation Restores Diaphragm Force and Metabolic Enzyme Activities in mdx Mice. *Antioxidants (Basel)* **6**, E101.

Burns DP, Canavan L, Rowland J, O'Flaherty R, Brannock M, Drummond SE, O'Malley D, Edge D & O'Halloran KD. (2018). Recovery of respiratory function in mdx mice co-treated with neutralizing interleukin-6 receptor antibodies and urocortin-2. *J Physiol* **596**, 5175-5197.

Burns DP & O'Halloran KD. (2016). Evidence of hypoxic tolerance in weak upper airway muscle from young mdx mice. *Respir Physiol Neurobiol* **226,** 68-75.

Burns DP, Rowland J, Canavan L, Murphy KH, Brannock M, O'Malley D, O'Halloran KD & Edge D. (2017b). Restoration of pharyngeal dilator muscle force in dystrophin-deficient (mdx) mice following co-treatment with neutralizing interleukin-6 receptor antibodies and urocortin 2. *Exp Physiol* **102,** 1177-1193.

Burns DP, Roy A, Lucking EF, McDonald FB, Gray S, Wilson RJ, Edge D & O'Halloran KD. (2017c). Sensorimotor control of breathing in the mdx mouse model of Duchenne muscular dystrophy. *J Physiol* **595,** 6653-6672.

Capogrosso RF, Mantuano P, Cozzoli A, Sanarica F, Massari AM, Conte E, Fonzino A, Giustino A, Rolland JF, Quaranta A, De Bellis M, Camerino GM, Grange RW & De Luca A. (2017). Contractile efficiency of dystrophic mdx mouse muscle: in vivo and ex vivo assessment of adaptation to exercise of functional end points. *J Appl Physiol (1985)* **122,** 828-843.

Carlson CG & Roshek DM. (2001). Adult dystrophic (mdx) endplates exhibit reduced quantal size and enhanced quantal variation. *Pflugers Arch* **442,** 369-375.

Carretta D, Santarelli M, Vanni D, Carrai R, Sbriccoli A, Pinto F & Minciacchi D. (2001). The organisation of spinal projecting brainstem neurons in an animal model of muscular dystrophy. A retrograde tracing study on mdx mutant mice. *Brain Res* **895,** 213-222.

Chaussenot R, Edeline JM, Le Bec B, El Massioui N, Laroche S & Vaillend C. (2015). Cognitive dysfunction in the dystrophin-deficient mouse model of Duchenne muscular dystrophy: A reappraisal from sensory to executive processes. *Neurobiol Learn Mem* **124,** 111-122.

De Bruin PF, Ueki J, Bush A, Khan Y, Watson A & Pride NB. (1997). Diaphragm thickness and inspiratory strength in patients with Duchenne muscular dystrophy. *Thorax* **52,** 472-475.

Ervasti JM. (2007). Dystrophin, its interactions with other proteins, and implications for muscular dystrophy. *Biochim Biophys Acta* **1772,** 108-117.

Gayraud J, Matecki S, Hnia K, Mornet D, Prefaut C, Mercier J, Michel A & Ramonatxo M. (2007). Ventilation during air breathing and in response to hypercapnia in 5 and 16 month-old mdx and C57 mice. *J Muscle Res Cell Motil* **28,** 29-37.

Gosselin LE, Barkley JE, Spencer MJ, McCormick KM & Farkas GA. (2003). Ventilatory dysfunction in mdx mice: impact of tumor necrosis factor-alpha deletion. *Muscle Nerve* **28,** 336-343.

Greising SM, Mantilla CB, Medina-Martínez JS, Stowe JM & Sieck GC. (2015). Functional impact of diaphragm muscle sarcopenia in both male and female mice. *Am J Physiol Lung Cell Mol Physiol* **309,** L46-52.

Greising SM, Mantilla CB & Sieck GC. (2016). Functional Measurement of Respiratory Muscle Motor Behaviors Using Transdiaphragmatic Pressure. *Methods Mol Biol* **1460,** 309-319.

Greising SM, Sieck DC, Sieck GC & Mantilla CB. (2013). Novel method for transdiaphragmatic pressure measurements in mice. *Respir Physiol Neurobiol* **188,** 56-59.

Grundy D. (2015). Principles and standards for reporting animal experiments in The Journal of Physiology and Experimental Physiology. *J Physiol* **593,** 2547-2549.

Hoffman EP, Brown RH & Kunkel LM. (1987). Dystrophin: the protein product of the Duchenne muscular dystrophy locus. *Cell* **51,** 919-928.

Hukins CA & Hillman DR. (2000). Daytime predictors of sleep hypoventilation in Duchenne muscular dystrophy. *Am J Respir Crit Care Med* **161,** 166-170.

Khan Y & Heckmatt JZ. (1994). Obstructive apnoeas in Duchenne muscular dystrophy. *Thorax* **49,** 157-161.

Khirani S, Ramirez A, Aubertin G, Boulé M, Chemouny C, Forin V & Fauroux B. (2014). Respiratory muscle decline in Duchenne muscular dystrophy. *Pediatr Pulmonol* **49,** 473-481.

Khurram OU, Fogarty MJ, Rana S, Vang P, Sieck GC & Mantilla CB. (2018a). Diaphragm muscle function following mid-cervical contusion injury in rats. *J Appl Physiol (1985)*.

Khurram OU, Fogarty MJ, Sarrafian TL, Bhatt A, Mantilla CB & Sieck GC. (2018b). Impact of aging on diaphragm muscle function in male and female Fischer 344 rats. *Physiol Rep* **6,** e13786.

Lewis P, Sheehan D, Soares R, Coelho AV & O'Halloran KD. (2016). Redox Remodeling Is Pivotal in Murine Diaphragm Muscle Adaptation to Chronic Sustained Hypoxia. *Am J Respir Cell Mol Biol* **55,** 12-23.

Lewis P, Sheehan D, Soares R, Varela Coelho A & O'Halloran KD. (2015). Chronic sustained hypoxia-induced redox remodeling causes contractile dysfunction in mouse sternohyoid muscle. *Front Physiol* **6,** 122.

Lidov HG. (1996). Dystrophin in the nervous system. *Brain Pathol* **6,** 63-77.

LoMauro A, D'Angelo MG, Romei M, Motta F, Columbo D, Comi GP, Pedotti A, Marchi E, Turconi AC, Bresolin N & Aliveri A. (2010). Abdominal volume contribution to tidal volume as an early indicator of respiratory impairment in Duchenne muscular dystrophy. *Eur Respir J* **35**, 1118-1125.

Lynch GS, Hinkle RT & Faulkner JA. (2001). Force and power output of diaphragm muscle strips from mdx and control mice after clenbuterol treatment. *Neuromuscul Disord* **11,** 192-196.

Mantilla CB, Seven YB, Hurtado-Palomino JN, Zhan WZ & Sieck GC. (2011). Chronic assessment of diaphragm muscle EMG activity across motor behaviors. *Respir Physiol Neurobiol* **177,** 176-182.

Mantilla CB, Seven YB & Sieck GC. (2014). Convergence of pattern generator outputs on a common mechanism of diaphragm motor unit recruitment. *Prog Brain Res* **209,** 309-329.

Mantilla CB, Seven YB, Zhan WZ & Sieck GC. (2010). Diaphragm motor unit recruitment in rats. *Respir Physiol Neurobiol* **173,** 101-106.

Mayer OH, Finkel RS, Rummey C, Benton MJ, Glanzman AM, Flickinger J, Lindström BM & Meier T. (2015). Characterization of pulmonary function in Duchenne Muscular Dystrophy. *Pediatr Pulmonol* **50,** 487-494.

Mead AF, Petrov M, Malik AS, Mitchell MA, Childers MK, Bogan JR, Seidner G, Kornegay JN & Stedman HH. (2014). Diaphragm remodeling and compensatory respiratory mechanics in a canine model of Duchenne muscular dystrophy. *J Appl Physiol* (1985) **116**, 807-815.

Medina-Martínez JS, Greising SM, Sieck GC & Mantilla CB. (2015). Semi-automated assessment of transdiaphragmatic pressure variability across motor behaviors. *Respir Physiol Neurobiol* **215,** 73-81.

Muntoni F, Torelli S & Ferlini A. (2003). Dystrophin and mutations: one gene, several proteins, multiple phenotypes. *Lancet Neurol* **2,** 731-740.

Nichols NL, Gowing G, Satriotomo I, Nashold LJ, Dale EA, Suzuki M, Avalos P, Mulcrone PL, McHugh J, Svendsen CN & Mitchell GS. (2013). Intermittent hypoxia and stem cell implants preserve breathing capacity in a rodent model of amyotrophic lateral sclerosis. *Am J Respir Crit Care Med* **187,** 535-542.

Nichols NL, Johnson RA, Satriotomo I & Mitchell GS. (2014). Neither serotonin nor adenosine-dependent mechanisms preserve ventilatory capacity in ALS rats. *Respir Physiol Neurobiol* **197,** 19-28.

Personius KE & Sawyer RP. (2006). Variability and failure of neurotransmission in the diaphragm of mdx mice. *Neuromuscul Disord* **16,** 168-177.

Phillips MF, Quinlivan RC, Edwards RH & Calverley PM. (2001). Changes in spirometry over time as a prognostic marker in patients with Duchenne muscular dystrophy. *Am J Respir Crit Care Med* **164,** 2191-2194.

Pinto ML, Tokunaga HH, Souccar C, Schoorlemmer GH & da Silva Lapa ReC. (2008). Loss of neuronal projections in the dystrophin-deficient mdx mouse is not progressive. *Brain Res* **1224,** 127-132.

Sawnani H, Thampratankul L, Szczesniak RD, Fenchel MC & Simakajornboon N. (2015). Sleep disordered breathing in young boys with Duchenne muscular dystrophy. *J Pediatr* **166,** 640-645.e641.

Sbriccoli A, Santarelli M, Carretta D, Pinto F, Granato A & Minciacchi D. (1995). Architectural changes of the cortico-spinal system in the dystrophin defective mdx mouse. *Neurosci Lett* **200,** 53-56.

Sekiguchi M, Zushida K, Yoshida M, Maekawa M, Kamichi S, Sahara Y, Yuasa S, Takeda S & Wada K. (2009). A deficit of brain dystrophin impairs specific amygdala GABAergic transmission and enhances defensive behaviour in mice. *Brain* **132,** 124-135.

Selsby JT, Ballmann CG, Spaulding HR, Ross JW & Quindry JC. (2016). Oral quercetin administration transiently protects respiratory function in dystrophin-deficient mice. *J Physiol* **594,** 6037-6053.

Seven YB, Mantilla CB & Sieck GC. (2014). Recruitment of rat diaphragm motor units across motor behaviors with different levels of diaphragm activation. *J Appl Physiol (1985)* **117,** 1308-1316.

Sieck GC, Ferreira LF, Reid MB & Mantilla CB. (2013). Mechanical properties of respiratory muscles. *Compr Physiol* **3,** 1553-1567.

Sieck GC & Fournier M. (1989). Diaphragm motor unit recruitment during ventilatory and nonventilatory behaviors. *J Appl Physiol (1985)* **66,** 2539-2545.

Smith PE, Edwards RH & Calverley PM. (1989). Ventilation and breathing pattern during sleep in Duchenne muscular dystrophy. *Chest* **96,** 1346-1351.

Stedman HH, Sweeney HL, Shrager JB, Maguire HC, Panettieri RA, Petrof B, Narusawa M, Leferovich JM, Sladky JT & Kelly AM. (1991). The mdx mouse diaphragm reproduces the degenerative changes of Duchenne muscular dystrophy. *Nature* **352,** 536-539.

Suresh S, Wales P, Dakin C, Harris MA & Cooper DG. (2005). Sleep-related breathing disorder in Duchenne muscular dystrophy: disease spectrum in the paediatric population. *J Paediatr Child Health* **41,** 500-503.

Vaillend C & Chaussenot R. (2017). Relationships linking emotional, motor, cognitive and GABAergic dysfunctions in dystrophin-deficient mdx mice. *Hum Mol Genet* **26,** 1041-1055.

Yiu EM & Kornberg AJ. (2008). Duchenne muscular dystrophy. *Neurol India* **56,** 236-247.

6. Additional information

Competing interests

The authors have no financial, professional or personal conflicts relating to this publication.

Author contributions

DPB: experimental design; acquisition of data; data and statistical analysis and interpretation of data; drafting of the original manuscript; KHM: ventilation during chemostimulation: acquisition of data; data analysis; EFL: *in vivo* studies: experimental design; KDO'H: experimental design; acquisition of data; data and statistical analysis and interpretation of data; drafting of the original manuscript. All authors contributed to the drafting and critical revision of the manuscript for important intellectual content. All authors have approved the final version of the manuscript and agree to be accountable for all aspects of the work. All persons designated as authors qualify for authorship, and all those who qualify for authorship are listed.

Funding

DPB and KHM were supported by funding from the Department of Physiology, UCC.

Acknowledgements

We are grateful to staff of the Biological Services Unit, University College Cork for animal care.

Translational perspective

Duchenne muscular dystrophy (DMD) is an X-linked fatal neuromuscular disease. Respiratory-related morbidity and mortality are widely recognized features of DMD, yet there is a considerable knowledge gap in respect of a comprehensive understanding of the neural control of breathing and respiratory-related behaviours in the human dystrophinopathies. The dystrophin-deficient *mdx* mouse is a widely used pre-clinical model of DMD. In young adult *mdx* mice, we examined inspiratory pressure-generating capacity across a range of ventilatory and non-ventilatory behaviours to explore inherent deficits and compensations that manifest in dystrophic disease. Our study reveals remarkable compensation in support of respiratory system performance, at least early in disease, despite evidence of profound diaphragm muscle weakness. Our data illustrate a capacity to preserve peak inspiratory pressure generation, despite respiratory muscle weakness and impaired neural recruitment of primary inspiratory muscles (diaphragm and intercostal muscles). Our findings point to a considerable reserve in the capacity of the respiratory system to perform a broad range of function, probably owing to recruitment of auxiliary muscles in support of peak respiratory-related performance. Peak inspiratory pressure generation is most relevant to protective reflexes related to airway maintenance and clearance, which is particularly relevant to neuromuscular (and neurodegenerative) conditions, given that dysphagic patients are at risk of obstructive airway events

during sleep, and aspiration pneumonia. It will be important to determine if similar compensation presents in DMD boys and if the progressive loss of respiratory performance with advancing disease relates to a decline or loss of compensatory mechanisms. Clinical assessment of auxiliary muscle control of breathing during maximal pressure-generating manoeuvres is clearly warranted (e.g. assessment of scalene, sternocleidomastoid and trapezius EMG activities and oesophageal pressure measurement during maximal sniff manoeuvres). Rehabilitative strategies focussed on auxiliary muscles that support inspiratory pressure generation may prove promising. Further delineation of the compensatory signature of the neuromuscular control system governing respiratory performance in animal models of DMD may provide insight into mechanisms that can be protected and/or further harnessed in the development of therapeutic strategies for DMD.

Table legends

Table 1. *Ex vivo* wild-type and *mdx* diaphragm muscle contractile kinetics

Definition of abbreviations: CT, contraction time; ½ RT, half-relaxation time; Smax, peak shortening; Vmax, peak shortening velocity; L_o, optimum length. Data are shown as mean ± SD and were statistically compared using two-tailed unpaired Student's *t* tests.

Table 2. Baseline respiratory parameters in anaesthetised wild-type and *mdx* mice

Definition of abbreviations: f_R, respiratory frequency; SpO_2, peripheral capillary oxygen saturation; $ETCO_2$, end-tidal carbon dioxide. Data are shown as mean ± SD and were statistically compared using two-tailed unpaired Student's *t* tests.

Table 3. Baseline respiratory parameters in anaesthetized wild-type and *mdx* mice before and during peak sustained efforts during airway occlusion

Definition of abbreviations: f_R, respiratory frequency; SpO_2, peripheral capillary oxygen saturation; T_i, inspiratory duration; TTP, time to peak sub-atmospheric pressure; Dia AUC, area under the curve of diaphragm integrated EMG signal (A.U. = arbitrary units); T3 EIC AUC, area under the curve of T3 external intercostal integrated EMG signal (A.U. = arbitrary units). Data are shown as mean ± SD and were statistically compared by repeated measures two-way analysis of variance (RMANOVA). * $P < 0.05$ compared with wild-type baseline; \$ $P < 0.05$, \$\$\$ $P < 0.001$ compared with wild-type obstruction.

Table 4. Baseline respiratory parameters in anaesthetized, vagotomized wild-type and *mdx* mice

Definition of abbreviations: f_R, respiratory frequency; V_T, tidal volume; V_E, minute ventilation; PIF, peak inspiratory flow; PEF, peak expiratory flow; $ETCO_2$, end-tidal carbon dioxide; SpO_2, peripheral capillary oxygen saturation. Data are shown as mean ± SD and were statistically compared using two-tailed unpaired Student's *t* tests.

Figure legends

Figure 1. *Ex vivo* wild type and *mdx* diaphragm muscle contractile function

A, B, C, and D, original traces of *ex vivo* diaphragm muscle twitch contraction (A), tetanic contraction (B), force-frequency relationship (C) and maximum unloaded shortening (D) for wild-type (WT; black) and *mdx* (grey) preparations. E, group data for diaphragm muscle twitch (P_t) and tetanic (P_o) force in WT (n = 8) and *mdx* (n = 9) mice. Tetanic force was measured following stimulation at 100 Hz *ex vivo*. Values are expressed as box and whisker plots (median, 25-75 percentile and scatter plot). Data were statistically compared by unpaired Student's *t* tests. **P* < 0.05, ****P* < 0.001 compared with corresponding WT value. F, group data (mean ± SD) for diaphragm muscle force-frequency relationship *ex vivo* in WT (open) and *mdx* (grey) preparations. Data were statistically compared by repeated measures two-way ANOVA (frequency x gene) followed by Bonferroni *post hoc* test. ***P* < 0.01, ****P* < 0.001 compared with corresponding WT value.

Figure 1.

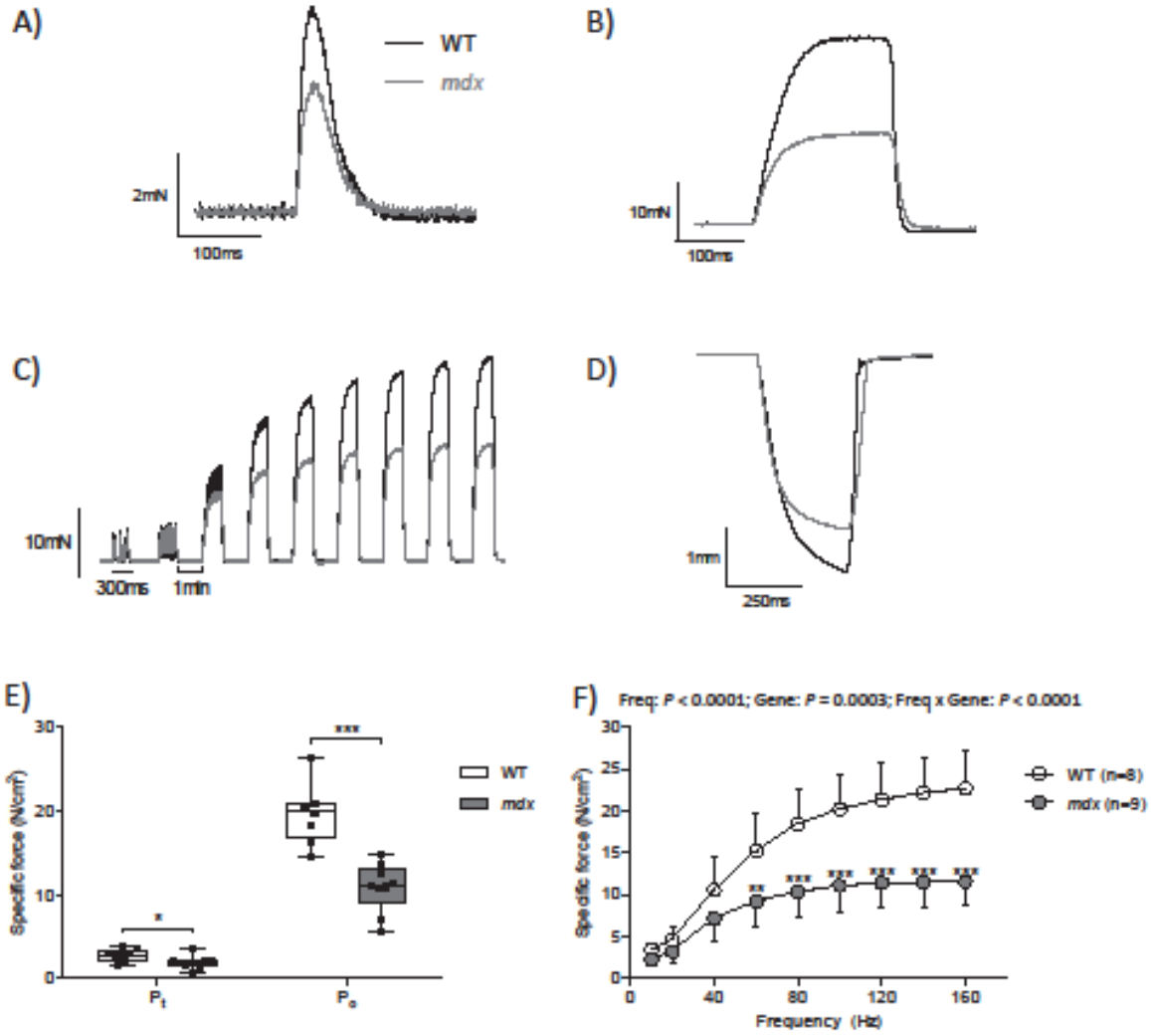

Figure 2. Ventilation in response to chemostimulation in conscious wild-type and *mdx* mice

A, representative respiratory flow traces during normoxia (21% O_2) and hypercapnic hypoxia (10% O_2 / 6% CO_2) in a wild-type (WT; black;) and *mdx* (grey) mouse; inspiration downwards. B, C, D and E, group data for respiratory frequency (B), tidal volume (C), minute ventilation (D) and mean inspiratory flow (E; V_T/T_i) during graded hypercapnia (2, 4 and 6% CO_2) and hypercapnic hypoxia (10% O_2 / 6% CO_2). Values are expressed as box and whisker plots (median, 25-75 percentile and scatter plot). Data were statistically compared by repeated measures two-way ANOVA.

Figure 2.

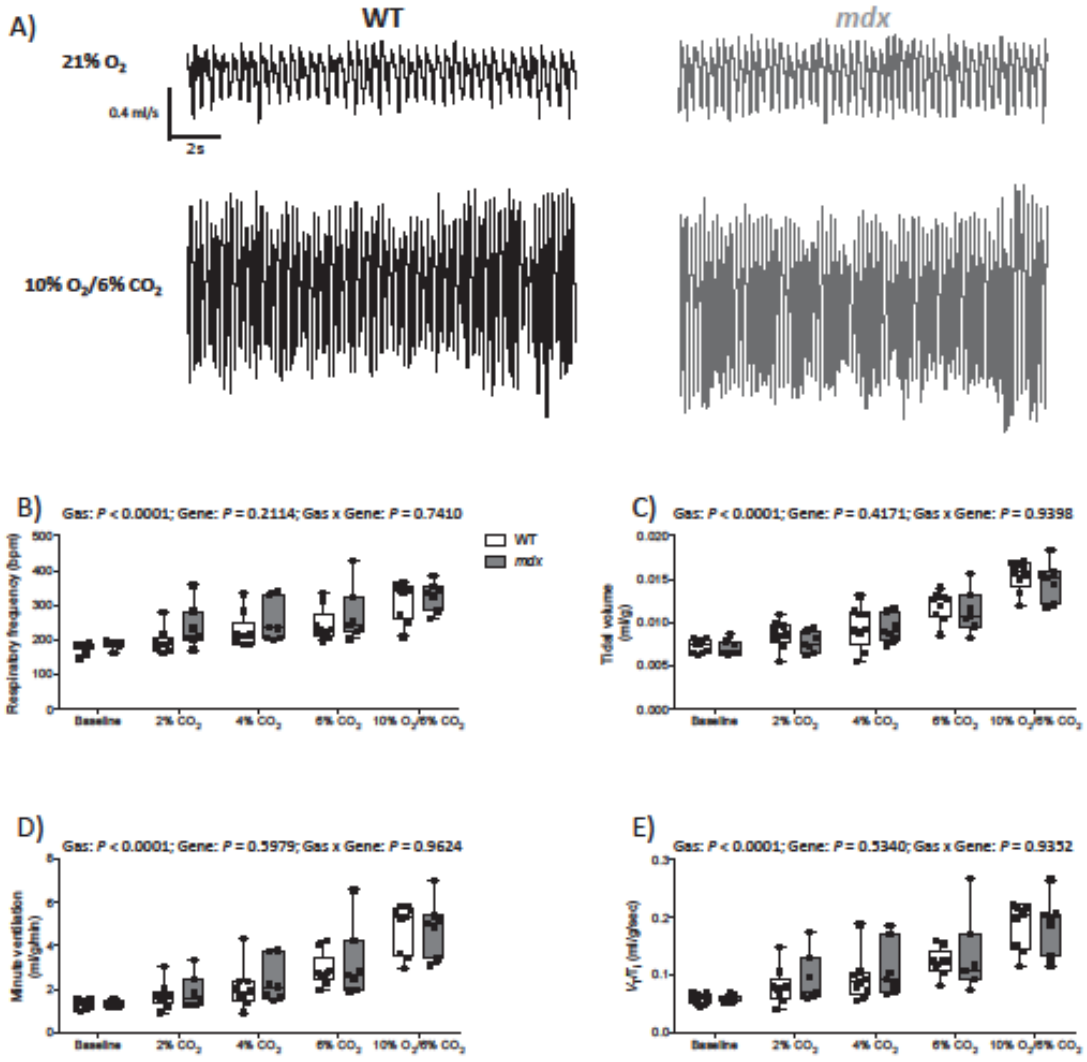

Figure 3. Oesophageal pressure and diaphragm EMG activity during ventilatory behaviours in anaesthetized wild-type and *mdx* mice

A, representative traces of oesophageal pressure and diaphragm (Dia) muscle raw and integrated (Int.) electromyogram (EMG) activity in a wild-type (WT; black) and *mdx* (grey) mouse during baseline (60% inspired O_2) and during an augmented breath (shaded). B and C, group data for oesophageal pressure (B) and diaphragm integrated EMG activity (C) during baseline, chemostimulation (15% O_2 / 5% CO_2) and augmented breaths for WT (n = 7-9) and *mdx* (n = 6-9) mice. Values are expressed as box and whisker plots (median, 25-75 percentile and scatter plot). Data were statistically compared by two-tailed unpaired Student's *t* tests. **P* = 0.025, ***P* = 0.0013 compared with corresponding WT values.

Figure 3.

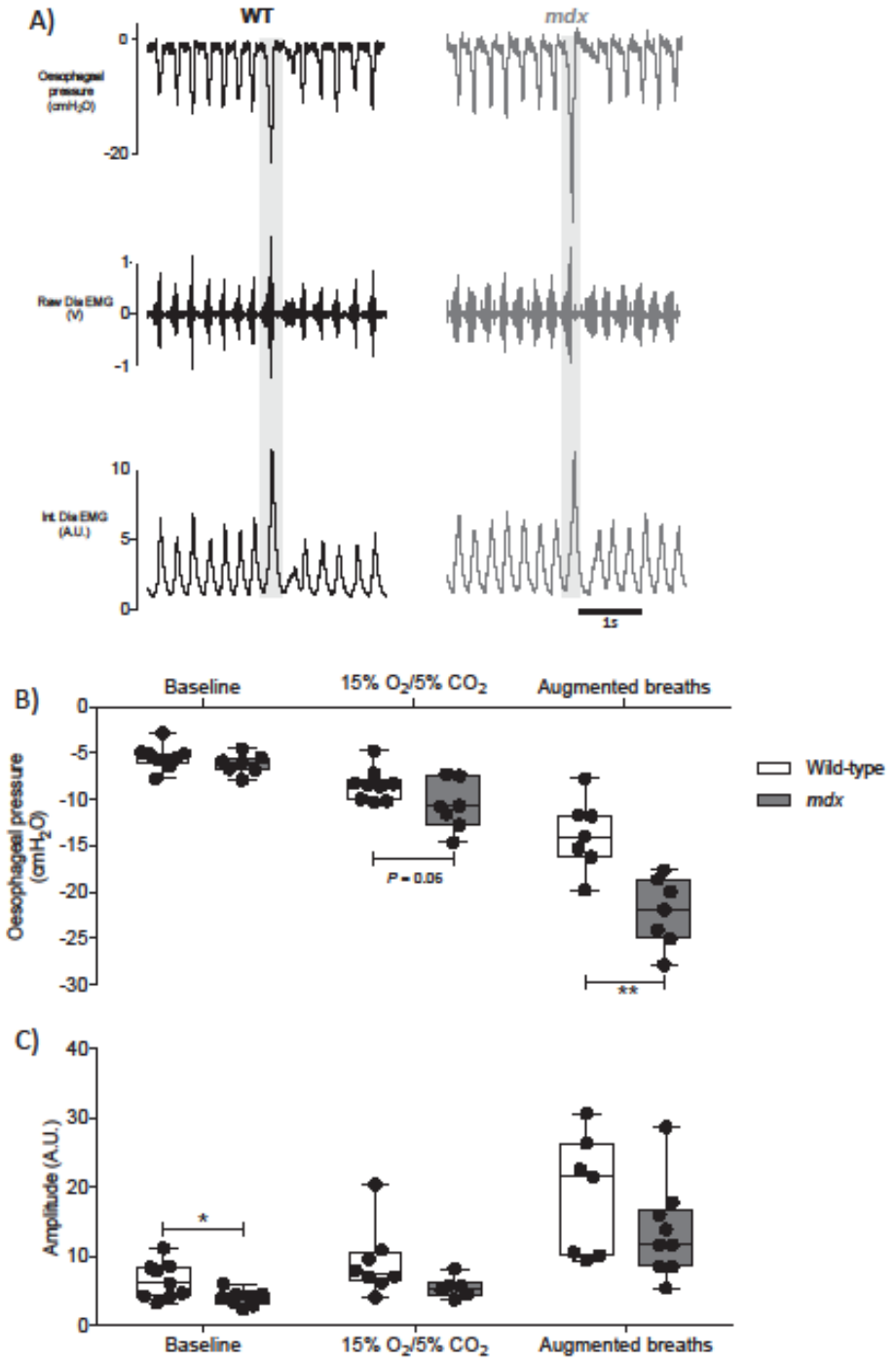

Figure 4. Oesophageal pressure and diaphragm and EIC EMG activities in anaesthetized wild-type and *mdx* mice: Original recordings

A, representative recordings of oesophageal pressure and diaphragm (Dia) and T3 external intercostal (T3 EIC) raw and integrated (Int.) electromyogram (EMG) activity in a wild-type (WT; black) and *mdx* (grey) mouse during baseline (F_iO_2 = 0.60) and protracted tracheal occlusion (~30-40 seconds). B, representative traces of oesophageal pressure and Dia and T3 EIC raw and Int. EMG activity in a WT and *mdx* mouse during baseline and peak inspiratory efforts (shaded) during a protracted tracheal occlusion.

Figure 4.

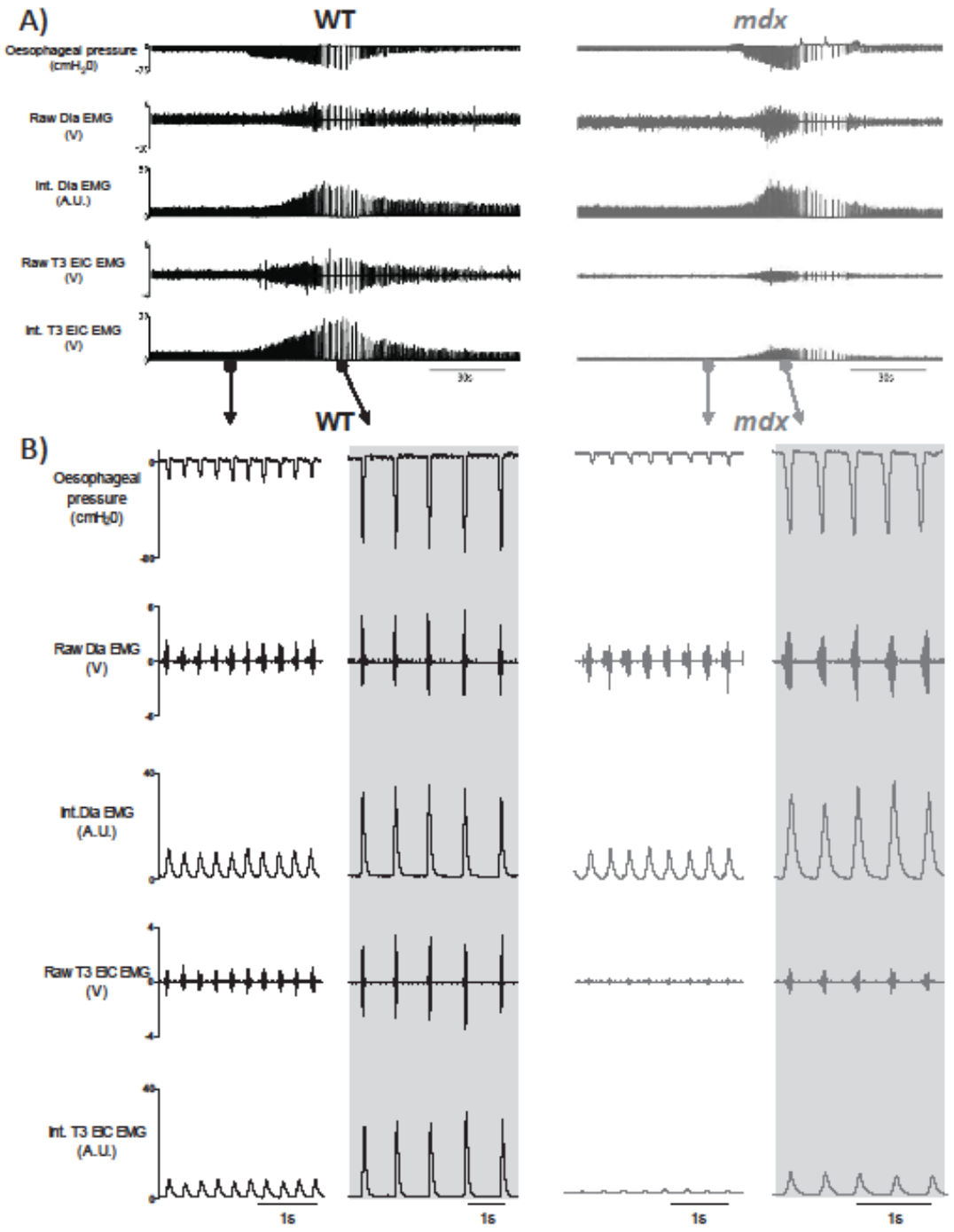

Figure 5. Oesophageal pressure and diaphragm and EIC EMG activities during tracheal occlusion in anaesthetized wild-type and *mdx* mice: Group data

A-C, group data for oesophageal pressure (A), diaphragm EMG activity (B) and T3 external intercostal (T3 EIC) EMG activity (C) during baseline conditions and during tracheal occlusion (average of 5 successive peak breaths) in WT (n=10) and *mdx* (n=10) mice. Values are expressed as box and whisker plots (median, 25-75 percentile and scatter plot). Data were statistically compared by repeated measures two-way ANOVA with Bonferroni *post hoc* test. **P* < 0.05; *****P* < 0.0001 compared with corresponding WT values.

Figure 5.

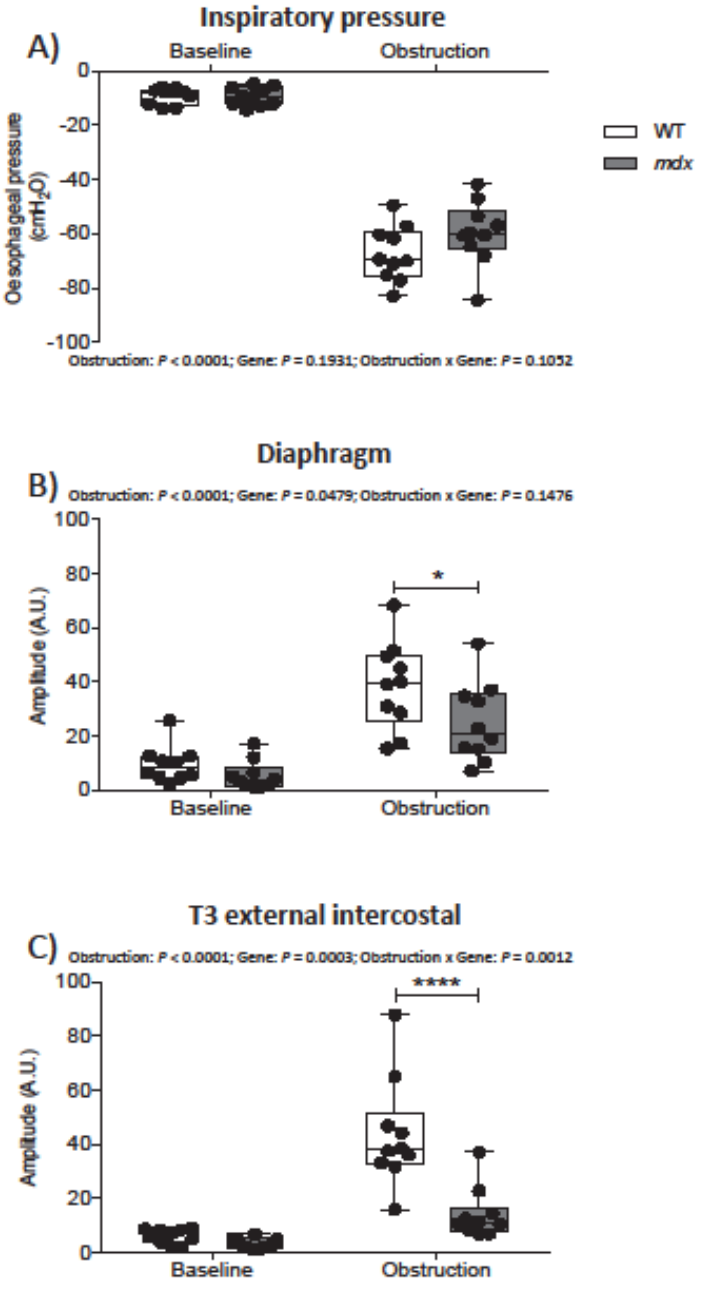

Figure 6. Tracheal airflow and diaphragm and EIC EMG activities in anaesthetized, vagotomized wild-type and *mdx* mice

A, representative recordings of tracheal airflow, tidal volume, raw and integrated (Int.) diaphragm (Dia) and T3 external intercostal (T3 EIC) electromyogram (EMG) activities for an anaesthetized wild-type (WT) mouse (black) and *mdx* mouse (grey) during baseline conditions (F_iO_2 = 0.60). B, C and D, group data for tidal volume (B), peak inspiratory flow (C) and peak expiratory flow (D) during baseline conditions and during spontaneous peak breaths during chemoactivation (F_iO_2 = 0.15 / F_iCO_2 = 0.06). E, diaphragm EMG activity during baseline and peak breaths. F, diaphragm EMG response (expressed as absolute change from baseline amplitude) during peak breaths. G, EIC EMG activity during baseline and peak breaths. H, EIC EMG activity (expressed as absolute change from baseline amplitude) during peak breaths. Values are expressed as box and whisker plots (median, 25-75 percentile and scatter plot). Data were statistically compared by repeated measures two-way ANOVA or two-tailed unpaired Student's *t* tests. **P* < 0.05; ***P* < 0.01 compared with corresponding WT values.

Figure 6.

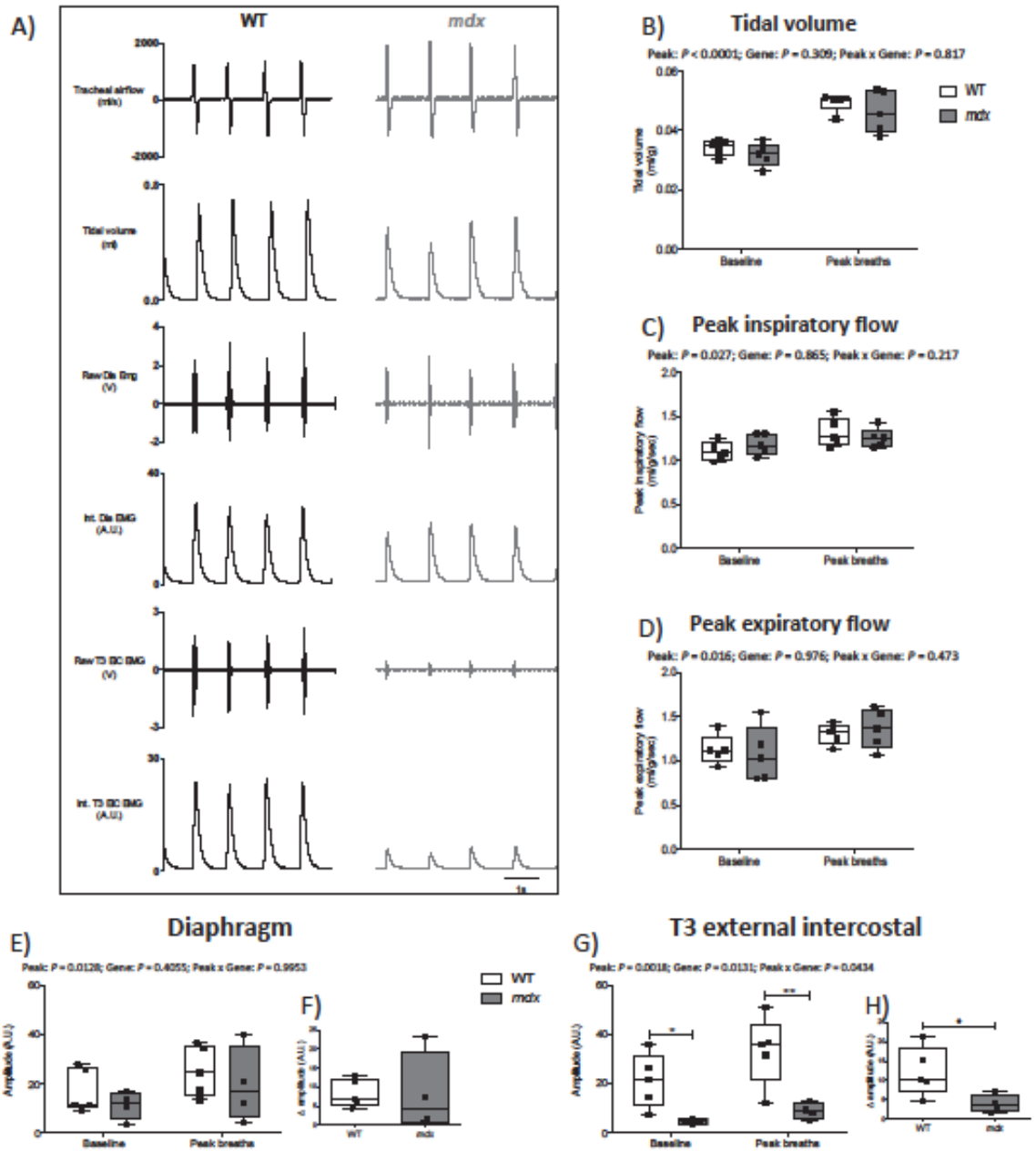

Table 1.

	Wild-type (n=8)	***mdx* (n=9)**	***P* (Student's *t* test)**
CT (ms)	17.3 ± 2.3	20.3 ± 2.6	0.0270
½ RT (ms)	19.6 ± 6.9	23.2 ± 4.3	0.2177
S_{max} (cm)	0.36 ± 0.07	0.26 ± 0.1	0.0386
S_{max} (L L_o^{-1})	0.36 ± 0.07	0.30 ± 0.13	0.3252
V_{max} (cm s^{-1})	4.1 ± 1.1	2.8 ± 1.3	0.0420
V_{max} (L_o s^{-1})	4.1 ± 1.1	3.3 ± 1.9	0.3373
L_o (cm)	1.0 ± 0.1	0.9 ± 0.2	0.1024

Table 2.

	Wild-type (n = 9)	***mdx* (n = 9)**	***P* (Student's *t* test)**
f_R (breaths min^{-1})	195 ± 11	230 ± 11	< 0.0001
SpO_2 (%)	97.2 ± 1.9	96.5 ± 2.0	0.4069
$ETCO_2$ (mmHg)	32.9 ± 3.3	30.3 ± 3.0	0.0966
Body mass (g)	24.9 ± 1.8	25.0 ± 2.3	0.9110

Table 3.

	Wild-type (n=10)		*mdx* (n=10)		*P* (RM two-way ANOVA)
	Baseline	**Obstruction**	**Baseline**	**Obstruction**	
f_R (breaths min^{-1})	217 ± 34	76 ± 18	227 ± 41	109 ± 32	Obstruction: *P* < 0.0001; Gene: *P* = 0.0802; Obstruction x Gene: *P* = 0.1962
SpO_2 (%)	95.1 ± 2.1	40.1 ± 9.5	95.8 ± 1.9	46.3 ± 9.1	Obstruction: *P* < 0.0001; Gene: *P* = 0.116; Obstruction x Gene: *P* = 0.2132
T_i (ms)	105 ± 15	144 ± 18	88 ± 14*	135 ± 15	Obstruction: *P* < 0.0001; Gene: *P* = 0.0441; Obstruction x Gene: *P* = 0.2073
TTP (ms)	58 ± 15	76 ± 11	50 ± 10	82 ± 13	Obstruction: *P* < 0.0001; Gene: *P* = 0.7911; Obstruction x Gene: *P* = 0.0438
Dia AUC (A.U.)	101 ± 76	585 ± 241	57 ± 56	382 ± 242$^{\$}$	Obstruction: *P* < 0.0001; Gene: *P* = 0.0582; Obstruction x Gene: *P* = 0.1349
T3 EIC AUC (A.U.)	65 ± 28	594 ± 215	34 ± 24	198 ± 131$^{\$\$\$}$	Obstruction: *P* < 0.0001; Gene: *P* < 0.0001; Obstruction x Gene: *P* = 0.0001

Table 4.

	Wild-type (n=10)	***mdx* (n=7)**	***P* (Student's *t* test)**
f_R (breaths min^{-1})	64 ± 19	60 ± 14	0.6932
V_T (ml g^{-1})	0.032 ± 0.005	0.032 ± 0.003	0.9800
V_E (ml g^{-1} min^{-1})	2.0 ± 0.7	1.9 ± 0.4	0.6343
PIF (ml g^{-1} s^{-1})	1.03 ± 0.16	1.15 ± 0.13	0.1345
PEF (ml g^{-1} s^{-1})	1.04 ± 0.18	1.08 ± 0.29	0.7207
$ETCO_2$ (mmHg)	53.2 ± 3.7	50.5 ± 6.1	0.2735
SpO_2 (%)	94.8 ± 2.5	94.1 ± 3.1	0.5821
Body mass (g)	24.8 ± 1.5	26.1 ± 0.8	0.0382

David P. Burns, PhD. David's primary research interest is the control of breathing in muscular dystrophy, with wider interests in cardiorespiratory physiology in animal models of disease. He received the Usha Award of the American Physiological Society, presented at the Experimental Biology 2017 meeting in Chicago and he was selected as one of three early career scientists working in Ireland to participate at the 68th Nobel Lindau meeting in Germany in 2018. This paper is the third in a series of studies published in *The Journal of Physiology* that were performed as part of his doctoral training at University College Cork, Ireland.